**Contract No:**

This document was prepared in conjunction with work accomplished under Contract No. DE-AC09-08SR22470 with the U.S. Department of Energy.

**Disclaimer:**

**Proceedings of PVP2008**
**2009 ASME Pressure Vessels and Piping Division Conference**
**July 27-30, 2009, Prague, Czech Republic**

**PVP2009-78086**

# Hydrogen Effects on Fracture Toughness of Type 316L Stainless Steel from 175 K to 425 K*

**Michael J. Morgan and Glenn K. Chapman**
**Savannah River National Laboratory, Aiken, SC 29808-0001**

## ABSTRACT

The effects of hydrogen on the fracture-toughness properties of Type 316L stainless steel from 175 K to 425 K were measured. Fracture-toughness samples were fabricated from Type 316L stainless steel forgings and hydrogen-charged with hydrogen at 34 MPa and 623 K for two weeks prior to testing. The effect of hydrogen on the J-Integral vs. crack extension behavior was measured at various temperatures by fracturing non-charged and hydrogen-charged samples in an environmental chamber. Hydrogen-charged steels had lower toughness values than non-charged ones, but still retained good toughness properties. The fracture-toughness values of hydrogen-charged samples tested near ambient temperature were about 70 % of non-charged values. For hydrogen-charged samples tested at 225 K and 425 K, the fracture-toughness values were 50% of the non-charged values. In all cases, fracture occurred by microvoid nucleation and coalescence, although the hydrogen-charged samples had smaller and more closely spaced microvoids. The results suggest that hydrogen effects on toughness are greater at 225 K than they are at ambient temperature because of strain-induced martensite formation. At 425 K, the hydrogen effects on toughness are greater than they are at ambient temperature because of the higher mobility of hydrogen.

## INTRODUCTION

Hydrogen damage in stainless steel has been shown to be temperature dependent [1, 2]. The most severe damage occurs at 220-280 K. This is shown in Fig. 1 which was taken from the work of George Caskey who compared the plastic strain to failure for hydrogen-charged tensile bars with the plastic strain to failure of non-charged tensile bars [1]. The effect of hydrogen on the plastic strain to failure was largest at about 220 K. Strain-induced martensite forms during low-temperature deformation of many austenitic stainless steels and possibly contributes to the low-temperature ductility minima in Fig. 1.

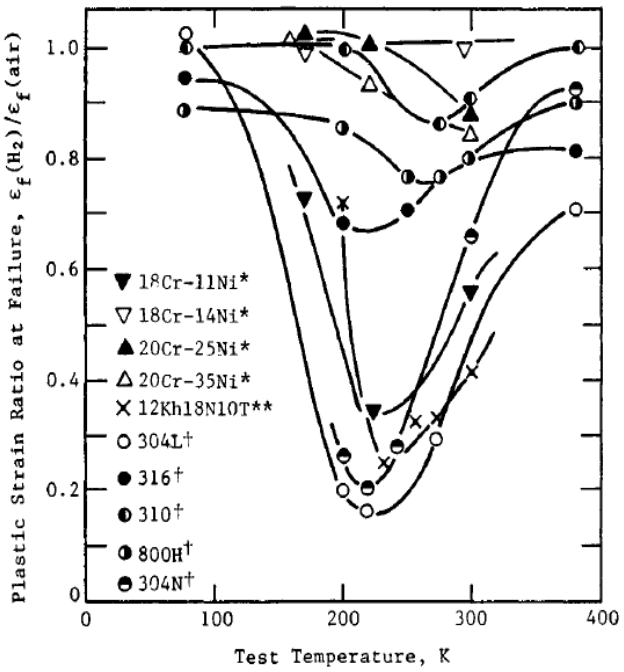


FIGURE 1. DUCTILITY MINIMA IN FE-CR-NI ALLOYS [1].

Tritium and deuterium gases are stored and processed at the Savannah River Site. In most plant systems, hydride technology is used to store, separate and process isotopes of hydrogen gas. Because these hydride vessels are thermally cycled to absorb and desorb deuterium and tritium gas, there is a need for mechanical property and fracture-toughness data on hydrogen exposed stainless steels as a function of temperature. The purpose of this study was to measure the fracture-toughness properties of Type 316L stainless steel at temperatures between 175 K and 425 K in the non-charged and hydrogen-charged conditions. Additionally, data from recently reported ambient temperature tests [3] are included.

## EXPERIMENTAL PROCEDURE

The composition and mechanical properties of the heat of Type 316L stainless steel used in this study is listed in Table I. The steel was supplied in the form of a 15 cm long by 3.8 cm diameter forward extruded cylindrical high-energy-rate forging. The microstructure of the forging is shown in Fig. 2.

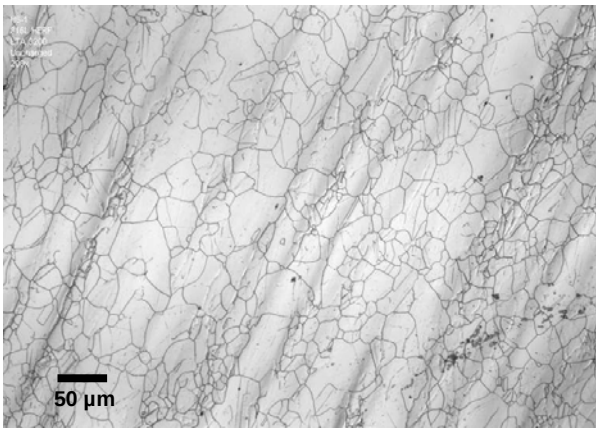


**FIGURE 2. MICROSTRUCTURE OF HERF 316L STAINLESS STEELS. SAMPLES WERE FABRICATED SO THAT THE CRACK PLANE PROPAGATED FROM RIGHT TO LEFT ABOVE. FORGING FLOW LINES ARE VISIBLE IN THE BACKGROUND OF THE IMAGE (60% NITRIC ACID ETCH).**

**TABLE I. COMPOSITION AND MECHANICAL PROPERTIES OF HERF 316L STAINLESS STEEL FORGING (WEIGHT %)**

| Material | Cr | Ni | Mn | P | Si | Co | Mo | C | S | N | O | Al | Cu |
|---|---|---|---|---|---|---|---|---|---|---|---|---|---|
| HERF 316L | 17.2 | 13.2 | 1.8 | .013 | .55 | - | 2.1 | .022 | .002 | .060 | .002 | - | .069 |

**NOTES:**
**HIGH ENERGY RATE FORGED FORWARD EXTRUDED CYLINDRICAL FORGING**
**DELTA FERRITE < 0.6%**
**INCLUSION RATING 1-1/2 D THIN**
**GRAIN SIZE 7**
**YIELD STRENGTH: 64.2 KSI; ULTIMATE STRENGTH: 107 KSI; ELONGATION: 40 %**

Arc-shaped fracture-mechanics specimens having the shape and dimensions shown in Fig. 3 were fabricated from the forgings and were fatigue pre-cracked. The fatigue crack was oriented so that the cracks would propagate across the forging flow lines in the radial direction (C-R). The samples were fatigue-cracked so that the crack-length to sample-width ratio was between 0.4 and 0.6. The size of the samples was chosen to be as large as possible to maximize constraint, but thin enough to diffuse hydrogen into the samples in reasonable times (~weeks) at temperatures that would not alter the microstructure. A finite-element analysis of the C-specimen showed that, for austenitic stainless steels, side grooves promote and establish near plane strain conditions at the crack front in sub-size specimens [4]. It was also found that a two-dimensional plane-strain analysis in conjunction with the standard American Society for Testing and Materials (ASTM)

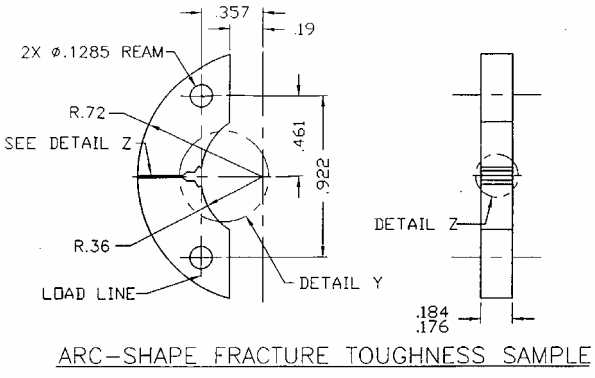


**FIGURE 3. SHAPE AND DIMENSIONS OF FRACTURE-TOUGHNESS SAMPLE. DIMENSIONS SHOWN ARE IN INCHES.**

was sufficient to determine the fracture-toughness values from side-grooved C-specimens [4].

Two sets of samples were prepared from each forging: Non-charged and hydrogen-charged. Non-charged samples were tested in the as-machined condition. Hydrogen-charged samples were prepared by equilibrating the machined samples with hydrogen gas at 34 MPa at 623 K for two weeks. The exposure conditions were chosen to saturate the samples throughout the thickness with hydrogen while minimizing any change to the steel microstructure. After charging, the samples were cooled in the presence of the hydrogen gas to below 273 K in about 15 minutes. The samples were stored in a freezer at 233 K prior to testing to minimize hydrogen off-gassing. The hydrogen content of the sample was calculated to be approximately 3700 atomic parts per million by using the solubility values of San Marchi, et al. [5].

The fracture-toughness properties were characterized by measuring the J-Integral vs. crack extension behavior in air at various temperatures using an environmental chamber capable of heating and cooling from 175 K to 425 K mounted to the mechanical testing machine (Fig. 4). Samples were tested using a crosshead speed of 0.002 mm/s while recording load, load-line displacement, and crack length. Crack length was monitored using an alternating DC potential drop system and guidelines described in ASTM E647-95 [6]. The J-Integral versus crack extension (J-R) curves were constructed from the data using ASTM E1820-99 [7]. The material fracture-toughness value was obtained from the intercept an offset from the crack tip blunting line with the J-R curve. These fracture-toughness values are reported as $J_Q$ values and not $J_{IC}$ values because they do not meet the size requirements of the ASTM E1820 standard [7]. However, finite-element analyses indicate that near plain-strain conditions are met at the crack tip at the point of crack extension where $J_Q$ is determined [4].

For this study, the crack tip blunting line was calculated from the ambient temperature yield strength and ultimate strength. A future study will investigate how the fracture-toughness values are affected by changes in the material yield strength with temperature. The crack length monitoring system was calibrated by measuring the length of the fatigue crack and the crack growth using microscopy measurements on the heat-tinted sample after the test, as shown in Fig. 5.

Three non-charged samples and three hydrogen-charged samples were tested at each test temperature: 175 K, 223 K, 273 K, Ambient (~298 K), 344 K, and 425 K. The temperature of the sample was monitored during the test using a thermocouple spot welded to the side face of the sample. Samples were equilibrated to the temperature of the environmental chamber for at least 30 minutes prior to testing. During testing, the samples were held within +/- 1.5 K of the test temperature. The J-Integral test took between twenty and forty minutes to complete. Hydrogen profiles in the samples before and after each test were calculated using a finite difference computer program and the solubility and diffusivity values for hydrogen in stainless steel [1, 8]. The test temperature had very little effect on the calculated hydrogen profile for the time it took to complete the test as shown by the calculated hydrogen profiles in Fig. 6.

Material microstructures were characterized using standard metallographic techniques, and fracture surfaces were characterized using scanning electron microscopy.

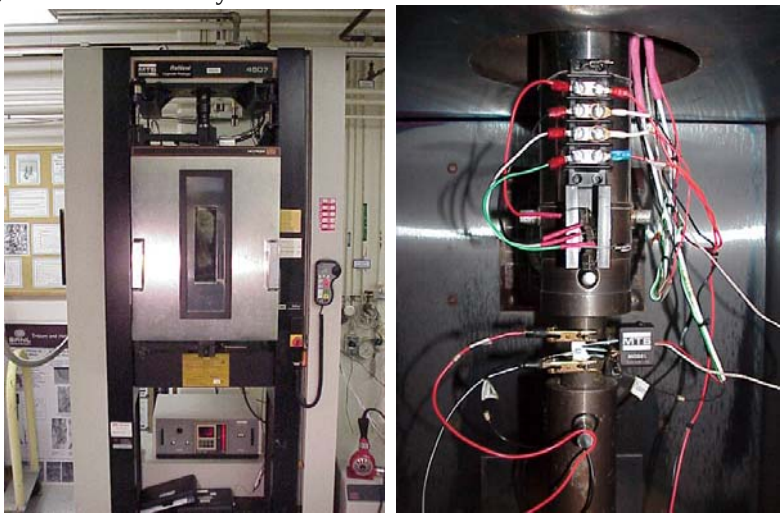

(a) (b)

**FIGURE 4. (A) MECHANICAL TESTING MACHINE WITH ENVIRONMENTAL CHAMBER AND (B) FRACTURE-TOUGHNESS SAMPLE WITH POTENTIAL- DROP LEADS AND THERMOCOUPLE.**

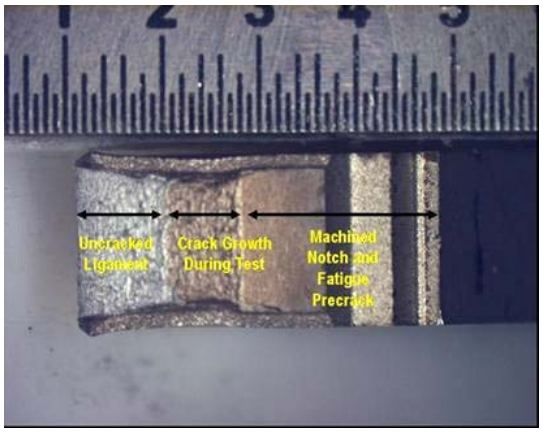


**FIGURE 5. HEAT-TINTED FRACTURE APPEARANCE AFTER J-R TEST.**

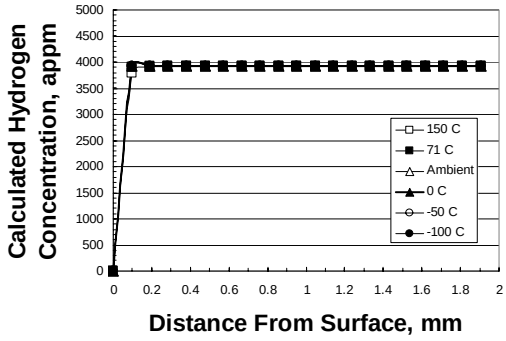


**FIGURE 6. CALCULATED HYDROGEN PROFILES FROM SURFACE TO CENTER LINE IN SPECIMENS DURING FRACTURE TEST.**

## RESULTS

Earlier results at ambient temperature indicate that Type 316L stainless steel has good fracture-toughness properties and is highly resistant to hydrogen effects on toughness [3]. Hydrogen-charged steels had lower toughness values than unexposed ones, but still retained good toughness properties. At ambient temperature, the non-charged steels had an average fracture-toughness value of 478 ± 60 kJ / sq. m. while the hydrogen-charged steels averaged 341 ± 27 kJ / sq. m.

Figure 7 shows the J-integral vs. crack extension (J-da) behavior for some of the non-charged samples tested at various temperatures in this study. The fracture-toughness value ($J_Q$) as determined by the intercept of the J-da curve with the offset to the crack blunting line is indicated in Fig. 7. There was a general trend toward decreasing fracture toughness and flatter J-da curves with increasing temperature. A similar trend was observed for the hydrogen-charged samples (Fig. 8).

Figure 9 shows the fracture-toughness values measured at all temperatures for non-charged and hydrogen-charged samples. Hydrogen-charged steels had lower toughness values than non-charged ones, but still retained good toughness properties. A plot of the average fracture-toughness value at each temperature is shown in Fig. 10. The general trend of decreasing fracture toughness with increasing temperature is evident from this figure. At the lowest temperature, 175 K, the hydrogen-charged samples had fracture-toughness values that were approximately 80% of the non-charged values. The fracture-toughness values of hydrogen-charged samples tested near ambient temperature were about 70 % of the values for non-charged samples. For hydrogen-charged samples tested at intermediately low temperatures (223 K and 425 K), the fracture-toughness values were about 50% of the non-charged values. From ambient temperature to 425 K, the toughness ratio declined steadily from ~70% to ~50%. Figure 11 shows the ratio of hydrogen-charged toughness to non-charged toughness over the entire temperature range.

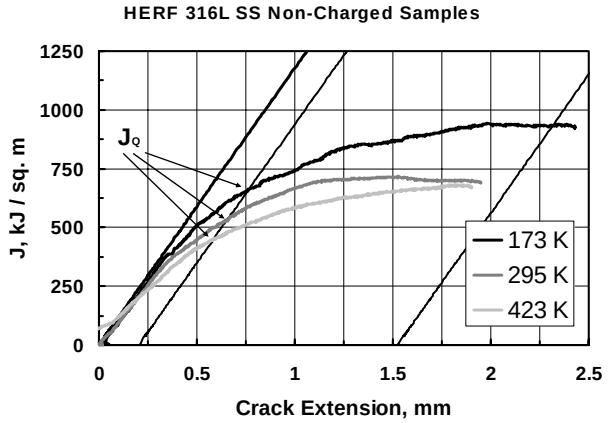


**FIGURE 7. TYPICAL J VS. CRACK-EXTENSION CURVES FOR NON-CHARGED SAMPLES TESTED AT 175 K, AMBIENT, AND 425 K.**

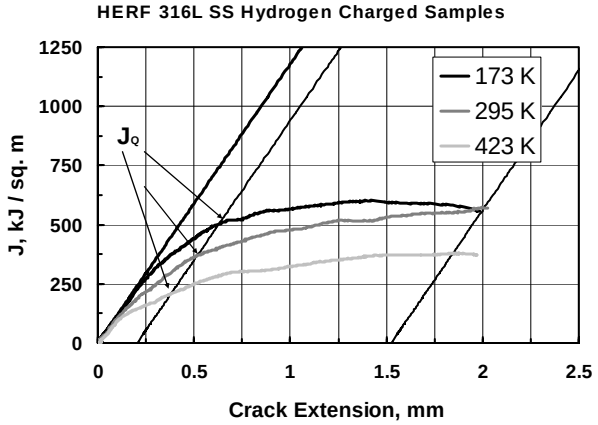


**FIGURE 8. TYPICAL J VS. CRACK EXTENSION CURVES FOR HYDROGEN-CHARGED SAMPLES TESTED AT 175 K, AMBIENT, AND 425 K.**

Hydrogen had relatively minor effects on fracture modes in this steel. At all temperatures, the fracture mode was by microvoid nucleation and growth. Crack propagation occurs by microvoids nucleating at nonmetallic inclusions in the steel in the high strain field ahead of the crack. The voids grow under increasing strain until the material between voids fails under the increasing strain, sometimes by void sheet formation. Figure 12 shows the high temperature (425 K) fracture mode for non-charged and hydrogen-charged samples. There was a higher density of microvoids on the fracture surface for hydrogen-charged samples than for non-charged samples.

At lower temperatures (175 K and 223 K), the microvoids on the fracture surfaces were less distinct than they were at higher temperatures. Notice in Fig. 13, that for samples tested at 175 K, the microvoids are more smeared out than they are at 425 K (Fig. 12). Also, there appeared to be a slightly different mechanism of fracture for hydrogen charged samples tested at low temperature. Notice in Fig. 13(b) and Fig. 14 that the larger voids appear to link up by void sheet formation when hydrogen is present. The evidence for this is the large numbers of very small microvoids between the larger microvoids. Also notice in Fig. 13(b) and Fig. 14 that there are patches of elongated features on the fracture surfaces of hydrogen-charged samples. These elongated features tended to be oriented in the forging direction.

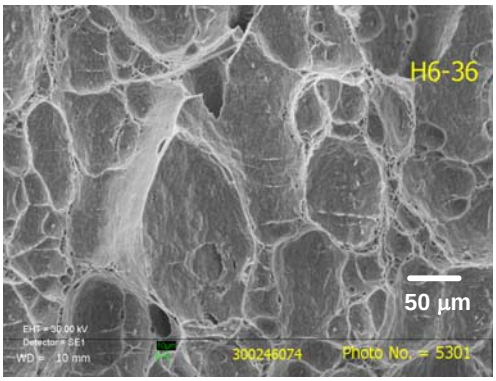


(A)

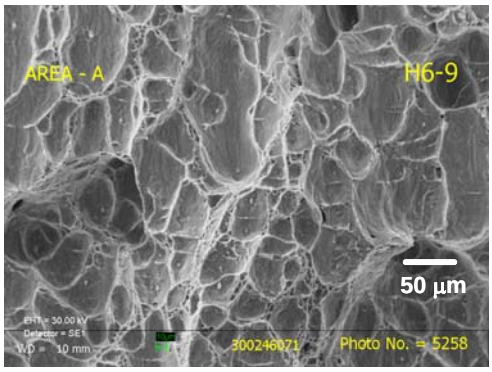


(B)

**FIGURE 12. FRACTURE APPEARANCE FOR SAMPLES TESTED AT 425 K: (A) NON-CHARGED AND (B) HYDROGEN-CHARGED.**

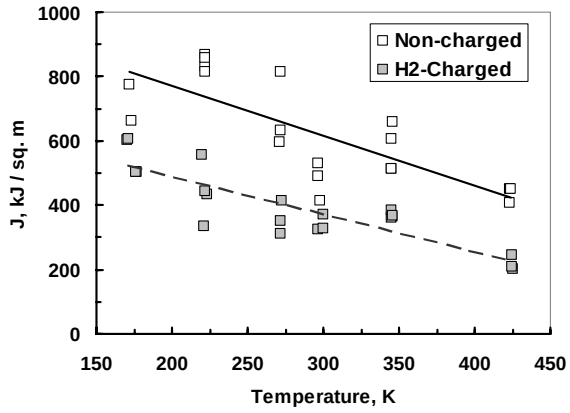


**FIGURE 9. J-INTEGRAL FRACTURE-TOUGHNESS VALUES FOR NON-CHARGED AND HYDROGEN-CHARGED SAMPLES FROM 175 K TO 425 K.**

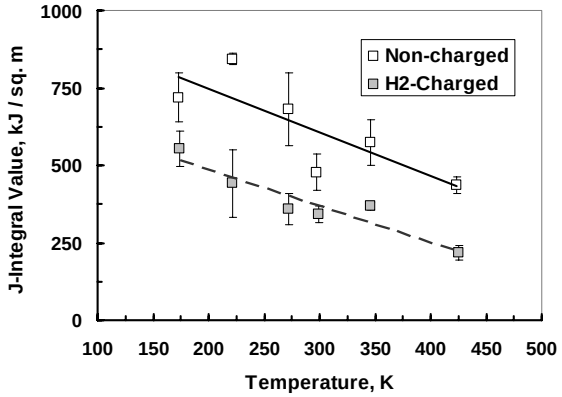


**FIGURE 10. AVERAGE J-INTEGRAL FRACTURE-TOUGHNESS VALUES FOR NON-CHARGED AND HYDROGEN-CHARGED SAMPLES FROM 175 K TO 425 K.**

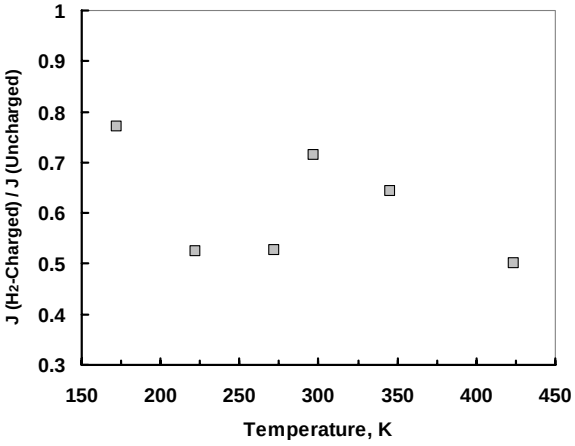


**FIGURE 11. RATIO OF J-INTEGRAL VALUES FOR HYDROGEN-CHARGED SAMPLES TO VALUES FOR NON-CHARGED SAMPLES FROM 175 K TO 425 K.**

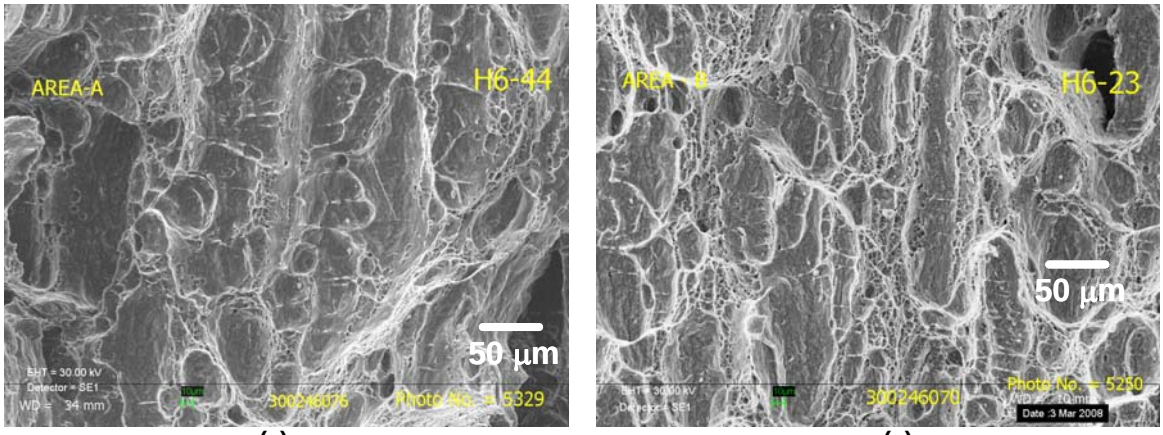


(A) (B)

**FIGURE 13. FRACTURE APPEARANCE FOR SAMPLES TESTED AT 175 K: (A) NON-CHARGED AND (B) HYDROGEN-CHARGED.**

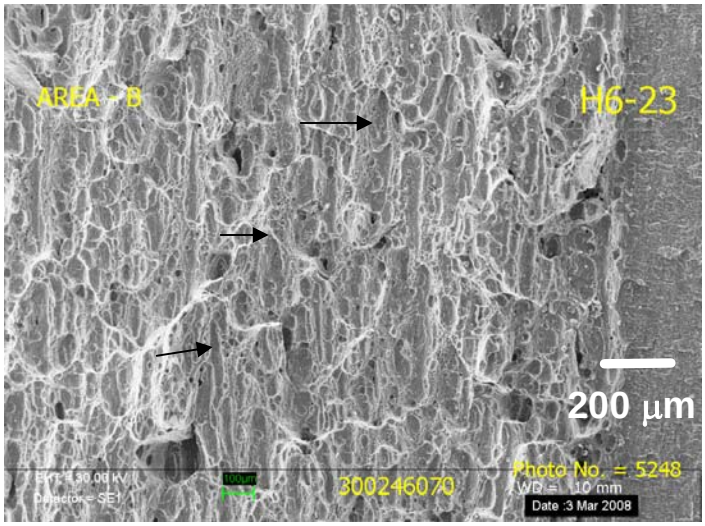


**FIGURE 14. ELONGATED FEATURES ON FRACTURE SURFACE OF HYDROGEN-CHARGED SAMPLE TESTED AT 175 K (SEE ARROWS).**

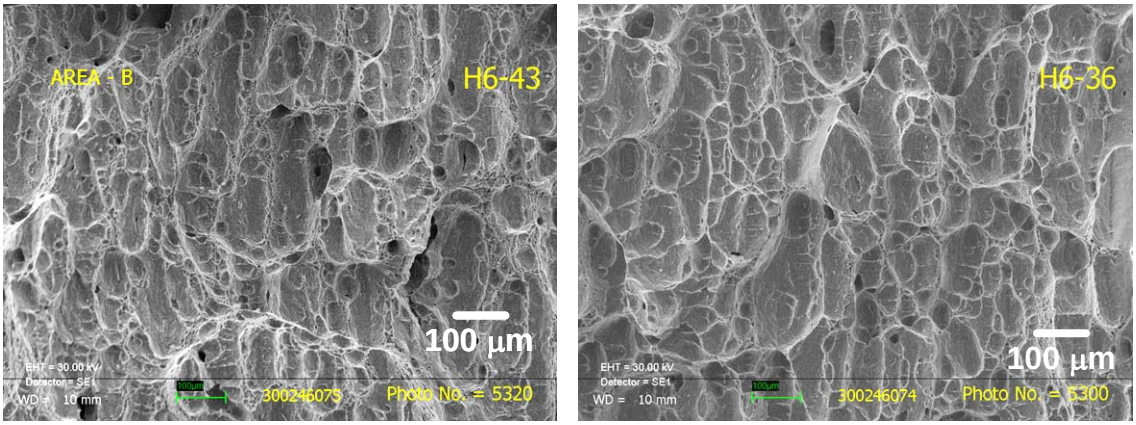


223K 425 K

**FIGURE 15. FRACTURE APPEARANCE FOR NON-CHARGED SAMPLES AT 223 K AND 425 K.**

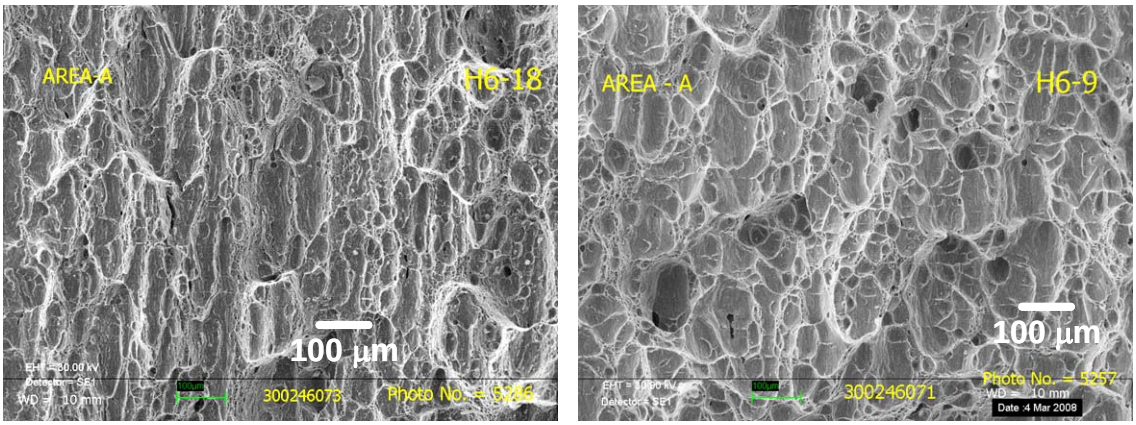


**223 K** **425 K**

**FIGURE 16. FRACTURE APPEARANCE FOR HYDROGEN-CHARGED SAMPLES AT 223 K AND 425 K.**

## DISCUSSION

The data above indicate two general areas of discussion: (1) Effect of temperature on fracture toughness and fracture modes of non-charged Type 316L stainless steel and (2) Effect of temperature and hydrogen on fracture toughness and fracture modes of this steel.

The fracture-toughness properties of non-charged Type 316L stainless steel have been shown to decrease with increasing temperature (Figs. 7 & 10). This is somewhat surprising because handbook data indicate that the yield strength of this increases with decreasing temperature [9] and fracture toughness usually decreases with increasing yield strength. Although the mechanical properties of this steel were not part of this study, they are planned for a future study. However, the fracture-toughness trends as a function of temperature are consistent with mechanical-property and Charpy-impact data trends from stainless steel handbook and literature data. For example, the Stainless Steel Handbook [9] lists typical mechanical properties of a number of austenitic stainless steels. For Type 316 stainless steel, yield strength and ultimate strength increase with decreasing temperature below 293 K. Surprisingly, in the same temperature range, elongation increases from 60% at 293 K to 87% at 223 [9]. Charpy- impact toughness also increases with decreasing temperature [9]. Furthermore, another study shows that elongation of non-charged and hydrogen-charged Type 316 stainless steel bar stock increases along with yield strength and ultimate strength at low temperatures [10]. The increase in toughness and elongation with increasing yield strength apparently result from the fact that the plastic deformation behavior of meta-stable austenitic stainless steels changes from slip at high temperature to deformation dominated by martensitic transformation at low temperature [11, 12]. This fundamental change in the plastic deformation behavior of Type 316L stainless steel with temperature is the most likely reason for the increase in fracture toughness with decreasing temperature seen in this study.

The change in plastic deformation behavior with temperature also affects the fracture mode as shown in Fig. 15. Type 316 stainless steel typically fails by nucleation, growth, and coalescence of microvoids [13-14]. When the material is deformed, inclusions and second-phase particles fracture or de-cohere from the matrix [14]. The resulting voids grow and their eventual coalescence leads to fracture. In stainless steels, there generally are two classes of voids on the fracture surface – one around large inclusions (like MnS or $Al_2O_3$), the other around small carbides. Large inclusions are often weakly bonded and initiate voids easily. As these voids grow, the material between the voids is severely strained. This eventually leads to breakage or de-cohesion of the strong and well bonded small particles by void sheet formation [14]. Figure 15 indicates that at low temperature the larger voids link up by void sheets; whereas at higher temperature they appear to link up by void growth. Because tensile strength decreases with increasing temperature in Type 316L stainless steels [10, 11, 15], the linking up of voids would be easier at higher temperature because the tensile strength of the ligament between growing microvoids would be lower. Crack advance occurs when a significant number of microvoids link up across the crack front. The fact that the J-da curves of Fig. 7 tend to flatten out with increasing temperature is consistent with this idea.

How did temperature and hydrogen affect fracture toughness and fracture modes of this steel? The fracture-toughness values of hydrogen-charged samples tended to decrease with increasing temperature, just as they did for non-charged samples (Figs. 9-10). This study also suggests that the relative effect of hydrogen on the fracture toughness of Type

316L stainless steel appears to be temperature dependent (Fig. 11). The most severe damage occurs at 223 K and 425 K. The fracture-toughness values of hydrogen-charged samples tested near ambient temperature were about 70 % of non-charged values. For hydrogen-charged samples tested at 223 K and 425 K, the fracture-toughness values were 50% of the non-charged values. This data seem to be roughly consistent with Caskey's observations on stainless steel ductility and hydrogen effects [1].

Caskey attributed the ductility minima of Fig. 1 in hydrogen-exposed Fe-Cr-Ni alloys to the formation of strain-induced martensite [1, 11]. The less stable alloys were more affected by hydrogen. However, the picture is more complicated for data from fracture-toughness studies as a function of temperature. First of all, the yield strength and plastic deformation behavior of the steel are affected by temperature as was discussed above for non-charged samples.

Another complicating factor in interpreting the combined effect of temperature and hydrogen on fracture toughness is that temperature affects how tightly hydrogen is bound to microstructural defects as well as how fast hydrogen can diffuse through the lattice. Assuming that a critical amount of hydrogen will cause fracture at a critical value of stress or strain, hydrogen embrittlement will be highest when the right balance between diffusivity and trapping is reached. When the temperature is too low, the driving force for stress assisted diffusion of hydrogen to crack tips will be two low and there may not be enough hydrogen released by thermal activation from lattice traps. When the temperature is too high, thermal activation will make it more difficult for the critical amount of hydrogen to accumulate at crack tips and lattice defects.

Hydrogen had subtle effects on the fracture mechanism at all temperatures. Figures 12-16 show the difference in fracture modes for samples tested at high and low temperature. The higher density of microvoids on the fracture surfaces of hydrogen-charged samples tested at high temperature (Fig. 12) suggests that hydrogen lowers the particle-matrix interfacial strength and makes microvoid nucleation easier. For samples tested between 175 K and 223 K, the microvoids on the fracture surface were less distinct. Notice in Fig. 13 that, for non-charged samples, the microvoids are more smeared out than they are at 425 K. Also, there appeared to be a different fracture mode for hydrogen charged samples at low temperature. Notice in Fig. 13(b) and Fig. 14 that the larger voids appeared to link up by void sheet formation when hydrogen is present. The evidence for this is the large numbers of very small microvoids between the larger microvoids. Also notice in Figs. 13 & 14 that there are patches of elongated features on the fracture surface, particularly for hydrogen-charged samples (Fig. 13b). These elongated features are oriented in the forging direction and could simply indicate that microvoids grow more easily in the forging direction. Together, the presence of void sheets and elongated features on the fracture surfaces of hydrogen-charged samples suggest that hydrogen makes microvoid coalescence easier at low temperature.

One area that clearly needs further study is the role of transformed martensite on the hydrogen embrittlement process of the austenitic stainless steels. Type 316L stainless steel will transform to martensite under strain at low temperature [11] and the elongated features describe above as enhanced void coalescence might actually be separation along the austenite-martensite interfaces.

More work is planned, including fractography and metallography to confirm role of strain-induced martensite on the fracture behavior of austenitic stainless steels. In addition, fracture tests on Types 304L and 21-6-9 stainless steels will be conducted to elucidate the effect of temperature on the fracture-toughness properties of a variety of hydrogen-charged stainless steel alloys.

## CONCLUSIONS

**1.** The fracture toughness of Type 316L stainless steel has been shown to be temperature dependent. The fracture-toughness values increased with decreasing temperature from 175 K to 425 K.

**2.** Hydrogen-charged Type 316L stainless steel had lower fracture-toughness values than non-charged steels at all temperatures from 175 K to 425 K. The fracture-toughness values of hydrogen-charged samples tested near ambient temperature were about 70 % of non-charged values. For hydrogen-charged samples tested at 223 K and 425 K, the fracture-toughness values were 50% of the non-charged values.

**3.** At high temperature, the higher density of microvoids on the fracture surface of hydrogen-charged samples suggests that hydrogen enhances microvoid nucleation. At low temperature, the presence of void sheets and elongated features on the fracture surface suggest and that hydrogen enhances microvoid coalescence.

## ACKNOWLEDGMENTS

The authors wish to thank Jack Durden and Mike Summer for their assistance with fractography and Andy Duncan for his discussions on the plastic deformation behavior of stainless steels. The author wishes to acknowledge the support from the U. S. Department of Energy (DOE) to the Savannah River National Laboratory (SRNL) under Contract No. DE-AC09-08SR22470.

## REFERENCES


[1]. G. R. Caskey, Jr., "Hydrogen Effects in Stainless Steels", Hydrogen Degradation of Ferrous Alloys, ed. J. P. Hirth, R. W. Oriani, and M. Smialowski, eds., (Park Ridge, NJ: Noyes Publication, 1985), p. 822.

[2]. Thorsten Michler, Arkadiy A. Yukhimchuk, and Joerg Naumann, “Hydrogen environment embrittlement testing at low temperatures and high pressures”, Corrosion Science, 50 (2008) 3519–3526.

[3]. M. J. Morgan, “Hydrogen Effects on the Fracture-Toughness Properties of Forged Stainless Steels”, Proceedings of PVP2008, 2008 ASME Pressure Vessels and Piping Division Conference, PVP2008-61390. July 27-31, 2008, Chicago, Illinois USA.

[4]. Y. Kim, Y. J. Chao, M. J. Pechersky, and M. J. Morgan, “C-Specimen Fracture Toughness Testing: Effect of Side Grooves and η Factor” Journal of Pressure Vessel Technology, 126, (2004), pp. 293-299.

[5]. C. San Marchi, B.P. Somerday and S.L. Robinson, “Permeability, Solubility and Diffusivity of Hydrogen Isotopes in Stainless Steels at High Gas Pressures”, International Journal of Hydrogen Energy, Volume 32, Issue 1, January 2007, 100-116.

[6]. ASTM E647-95a “Standard Test Method for Measurement of Fatigue Crack Growth Rates”, 1999 Annual Book of ASTM Standard Volume 3.01 Metals-Mechanical Testing; Elevated and Low-Temperature Tests; Metallography, American Society for Testing and Materials, 1999.

[7]. ASTM E1820-99 “Standard Test Method for Measurement of Fracture Toughness”, 1999 Annual Book of ASTM Standard Volume 3.01 Metals-Mechanical Testing; Elevated and Low-Temperature Tests; Metallography, American Society for Testing and Materials, 1999.

[8]. K. E. Kain, “Finite-Difference Program For Hydrogen Diffusion”, DP-1738, E. I. du Pont de Nemours & Co., Savannah River Laboratory, Aiken, SC 29808, March, 1987.

[9]. K. G. Brickner and J. D. Defilippi, “Mechanical Properties of Stainless Steels at Cryogenic Temperatures and at Room Temperature”, Handbook of Stainless Steels, eds. Donald Peckner and I. M. Bernstein, McGraw Hill, (New York 1977), Chapter 20.

[10]. C. San Marchi, B.P. Somerday, X. Tang, G.H. Schiroky, “Effects of alloy composition and strain hardening on tensile fracture of hydrogen-precharged type 316 stainless steels”, International Journal of Hydrogen Energy, 33 (2008), pp. 889-904.

[11]. G. R. Caskey, Jr., “Hydrogen Compatibility Handbook for Stainless Steels”, E. I. du Pont de Nemours & Co., Savannah River Laboratory, Aiken SC 29808, DP-1643.

[12]. Tryggve Angel, “Formation of Martensite in Austenitic Stainless Steels”, The Metallurgical Evolution of Stainless Steels, ed. F. B. Pickering, ASM (Metals Park, OH 1979) p. 402.

[13]. C. Ludwigson and J. A. Berger, “Plastic Behavior of Metastable Austenitic Stainless Steels, The Metallurgical Evolution of Stainless Steels, ed. F. B. Pickering, ASM (Metals Park, OH 1979) p. 413.

[14]. H. Riedel, “Fracture Mechanisms”, Materials Science and Technology – A Comprehensive Treatment, Vol. 6, Chapter 12, eds. R. W. Cahn, P. Haasen, and E. J. Kramer, VCH (New York 1993).

[15]. W. D. Klopp, Aerospace Structural Materials Handbook, Ferrous Alloys, Type 316/317, June, 1988.